

Two-color phase-of-the-phase spectroscopy in the multiphoton regime

M. A. Almajid, M. Zabel, S. Skruszewicz,* J. Tiggesbäumker, and D. Bauer†

Institut für Physik, Universität Rostock, 18051 Rostock, Germany

(Dated: March 12, 2022)

Momentum-resolved photoelectron emission from xenon in colinearly polarized two-color laser fields at above-threshold ionization conditions is studied both experimentally and theoretically. We utilize phase-of-the-phase spectroscopy as recently introduced by Skruszewicz *et al.*, Phys. Rev. Lett. 115, 043001 (2015) to analyze the dependence of the yields on the relative phase φ between the fundamental and second harmonic laser fields. The resulting phase-of-phase spectra feature a characteristic checkerboard pattern, which can analytically be described within the strong-field approximation.

PACS numbers: 32.80.Rm, 34.80.Qb, 33.60.+q

I. INTRODUCTION

The development of lasers has revitalized atomic, molecular, chemical, and optical physics. The interaction of intense laser pulses with matter gives rise to a wealth of phenomena that are nonlinear in both the laser intensity and the number of photons involved, examples being multiphoton ionization (MPI), above-threshold ionization (ATI), or tunneling ionization (see, e.g., [1] for a review). While for weak laser fields MPI could still be tackled in a perturbative fashion where each additionally absorbed photon requires the next-order, conventional perturbation theory becomes inadequate for stronger fields due to the lack of a small parameter and very pronounced AC-Stark effects [2]. Instead, the so-called strong-field approximation (SFA) (see, e.g., [1, 3] for a recent review) became the work horse of choice and particularly insightful when interpreted in terms of quantum orbits [1, 3]. For instance, ATI peaks separated in energy by $\hbar\omega$ can be understood as the interference of quantum orbits of electrons emitted in subsequent laser cycles (inter-cycle interference) while interfering quantum orbits originating from the same laser cycle (intra-cycle interference) lead to other features in photoelectron spectra (PES) [4], such as holographic side lobes [5, 6].

Patterns in the photoelectron spectra clearly depend on the laser pulse and the target. The dependency on the particulars of the laser field allow for the control of the ionization dynamics or the precise experimental characterization of the laser pulse [7]. The dependency on the target opens up the possibility to image the system employing its own electrons [8].

In this work, we do not consider the PES themselves but the *change* of the momentum-resolved yield as function of the relative phase φ between the ω and the 2ω component of a colinearly polarized two-color pulse with vector potential (in dipole approximation)

$$\mathbf{A}(t) = A_0(t) \left[\sin \omega t + \xi \sin(2\omega t + \varphi) \right] \mathbf{e}_z, \quad (1)$$

where ξ is a relative field amplitude, and $A_0(t)$ is the envelope of the laser pulse. Note that if the ratio of 2ω to ω component of the vector potential is ξ , the ratio of the corresponding electric field components is 2ξ because $\mathbf{E} = -\partial_t \mathbf{A}$. The ratio in intensities then is $(2\xi)^2$. Below we will consider $\xi = 0.05$, i.e., the 2ω component of the electric field is 10% of the fundamental, and the intensity ratio is 1%.

A plethora of two-color studies have been performed recently, with different combinations of laser frequencies and polarizations [9–25]. Important foreseeable applications of two-color fields are the efficient generation of THz radiation from plasmas [13] or the control of strong-field phenomena by steering the electron emission [26], for instance. Atoms and molecules in two-color fields are also interesting in themselves as they allow a deeper understanding of the ionization dynamics due to the high sensitivity of strong-field observables to the detailed shape of the electric field, which is modified by the relative phase φ on a sub-cycle time scale. Relative-phase dependent measurements are thus a more challenging, stringent test for theory and, perhaps most importantly, offer the possibility to distinguish coherent and incoherent contributions to PES or other observables. Here, “coherent” and “incoherent” mean that the ionization dynamics that lead to photoelectrons with a certain final momentum in PES do depend or do not depend on the precise shape of the electric field of the laser, and thus on the relative phase φ . The subcycle ionization dynamics in few-active electron systems such as atoms or small molecules are expected to be coherent in this sense while thermal emission from larger systems is expected to be incoherent. Before we aim at complex targets though, we need to understand the canonical, “text-book” phase-of-the-phase (PP) spectra originating from coherent electron emission. In Ref. [24], phase-of-phase spectra were found to show a typical structure of two overlapping clubs due to rescattering in strong laser fields. In this work we investigate phase-of-phase spectra at lower laser intensities, i.e., in the multiphoton ionization (MPI) regime.

The paper is organized as follows: The fundamental idea behind phase-of-the-phase spectroscopy is introduced and a generic experimental result for Xe is presented in Sec. II. Simulation results and the derivation of the ionization rate for a two-color pulse, both based on the SFA, are presented in Sec. III, followed by a discussion in Sec. IV. We briefly summarize and give an outlook in Sec. V.

* Present address: Institut für Optik und Quantenelektronik, Friedrich-Schiller-Universität Jena, Max-Wien-Platz 1, 07743 Jena, Germany

† Corresponding author: dieter.bauer@uni-rostock.de

Atomic units are used unless indicated otherwise. The dipole approximation is valid for the laser parameters under study and applied throughout.

II. EXPERIMENTAL RESULT AND PHASE-OF-THE-PHASE ANALYSIS

Details of the experimental setup to measure phase-sensitive signals from two-color laser pulse excitations of atoms and molecules has been described previously [24]. Briefly, a Ti:sapphire laser system produces near-infrared pulses of energy $E_L = 2.5$ mJ and $\lambda = 794$ nm with a pulse duration of 180 fs at a repetition rate of 1 kHz. To sculpture the pulses on the time scale of the electric field oscillation the fundamental is superimposed by a weak second harmonic field with an intensity ratio $I_{2\omega}/I_\omega = 0.01$. The temporal overlap between fundamental and second harmonic is controlled by birefringent calcite crystals and two glass wedges. Additional wave plates are used to align the polarization axes parallel to each other. The wedges are mounted on piezo-driven motors to achieve sub-cycle control over the relative phase φ between ω and 2ω component. A concave silver-mirror with a focal length of 250 mm focuses the pulses into the interaction region of a homebuilt velocity map imaging (VMI) electron spectrometer [27], giving pulse intensities of $I_\omega \simeq 5 \times 10^{13}$ W cm $^{-2}$. Rare gases enter as an effusive beam from a nearby capillary.

Figure 1 shows a typical snapshot of the VMI screen for such a two-color experiment on xenon atoms. ATI rings and the previously studied “carpet” structure [28] are clearly visible. However, because the 2ω component is just a weak perturbation, no big changes are seen on the VMI screen with the naked eye when the relative phase φ is changed. The idea behind phase-of-the-phase spectroscopy is to study systematically the *change* in the photoelectron yield as a function of the relative phase φ (or any other periodic parameter, e.g., the carrier-envelope phase [29]). Assuming that the momentum-resolved yield $Y(\mathbf{p}, \varphi)$ behaves predominantly as

$$Y(\mathbf{p}, \varphi) \simeq Y_0(\mathbf{p}) + \Delta Y_1(\mathbf{p}) \cos[\varphi + \Phi_1(\mathbf{p})] \quad (2)$$

for most final photoelectron momenta \mathbf{p} , the change in the yield can be characterized by just two functions of \mathbf{p} : the relative phase contrast (RPC) $\Delta Y_1(\mathbf{p}) \geq 0$ and the phase of the phase (PP) $\Phi_1(\mathbf{p}) \in [-\pi, \pi)$ that tells us whether the yield changes, e.g., $\pm \cos$ -like with φ or $\pm \sin$ -like. Technically, phase of phase and relative phase contrast can be quickly determined by fast-Fourier-transforming $Y(\mathbf{p}, \varphi)$ with respect to φ for each \mathbf{p} . The yield may actually change with twice the relative phase for certain final momenta \mathbf{p} , i.e., $\sim \Delta Y_2(\mathbf{p}) \cos[2\varphi + \Phi_2(\mathbf{p})]$. In fact, this is the case in leading order $O(\xi^2)$ for electron emission perpendicular to the polarization direction because $\Delta Y_1 = 0$ there. However, in this work we limit our discussions to the fundamental PP Φ_1 , i.e., to order $O(\xi)$, as will be shown in Section III below.

Figure 2 shows the experimental RPC and PP spectra for xenon, determined from a series of snapshots for varied relative phase φ like the one in Fig. 1. For a fixed relative phase

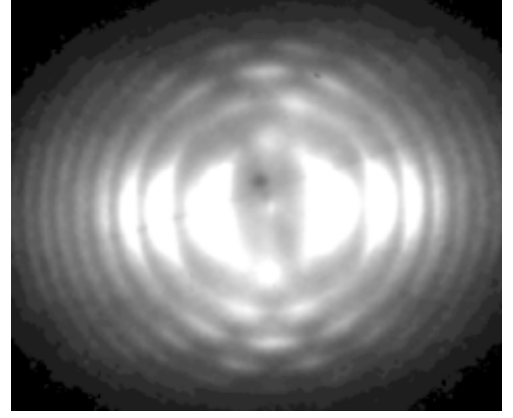


FIG. 1. Screenshot of the VMI detector during a colinearly polarized two-color experiment with Xe. Laser polarization in horizontal direction. Laser parameters are given in the text. ATI rings separated by $\hbar\omega$ in energy and the “carpet” structure [28] are clearly visible.

the average of 10000 PES is taken. The relative phase is sampled in steps of $\simeq 2\pi/70$. A checkerboard pattern in the PP along the ATI rings is clearly visible. The color coding can be cyclically shifted because only the change in the relative phase is controlled in the experiment, not its absolute value. We chose the color-coding such that the checkerboard pattern is red and blue, representing $\pm \sin$ -like changes in the yield $Y(\mathbf{p}, \varphi)$ according to the pulse form (2) assumed in the theoretical analysis.

III. THEORY

We apply the SFA for the so-called direct electrons, i.e., those that do not rescatter at the parent ion. In length gauge, the SFA matrix element reads [1, 3]

$$M_{\mathbf{p}}^{(\text{SFA})} = -i \int_{-\infty}^{\infty} \langle \Psi_{\mathbf{p}}^{\text{GV}}(t) | \mathbf{r} \cdot \mathbf{E}(t) | \Psi_0(t) \rangle dt \quad (3)$$

where

$$|\Psi_{\mathbf{p}}^{\text{GV}}(t)\rangle = e^{-iS_{\mathbf{p}}(t)} |\mathbf{p} + \mathbf{A}(t)\rangle \quad (4)$$

is a Gordon-Volkov (GV) state, i.e., a solution to the time-dependent Schrödinger equation $i|\dot{\Psi}_{\mathbf{p}}^{\text{GV}}(t)\rangle = [\mathbf{p}^2/2 + \mathbf{r} \cdot \mathbf{E}(t)]|\Psi_{\mathbf{p}}^{\text{GV}}(t)\rangle$ without binding potential but laser only, $|\Psi_0(t)\rangle = \exp(iI_{\text{p}}t)|\Psi_0(0)\rangle$ is the initial bound state, and

$$S_{\mathbf{p}}(t) = \frac{1}{2} \int_0^t [\mathbf{p} + \mathbf{A}(t')]^2 dt' \quad (5)$$

is the Coulomb-free, classical action. In dipole approximation, the PES $|M_{\mathbf{p}}^{(\text{SFA})}|^2$ is azimuthally symmetric about the laser polarization axis in \mathbf{e}_z direction. For illustration, PES calculated with the SFA for laser intensity $I = 5 \times 10^{13}$ W/cm 2 , $\lambda = 800$ nm ($\omega = 0.057$), 20-cycle \sin^2 pulse, $\xi = 0.05$, relative phases $\varphi = 0, \pi/2, 3\pi/2$, and $I_{\text{p}} = 0.445$ (Xe) are shown in Fig. 3. The initial state

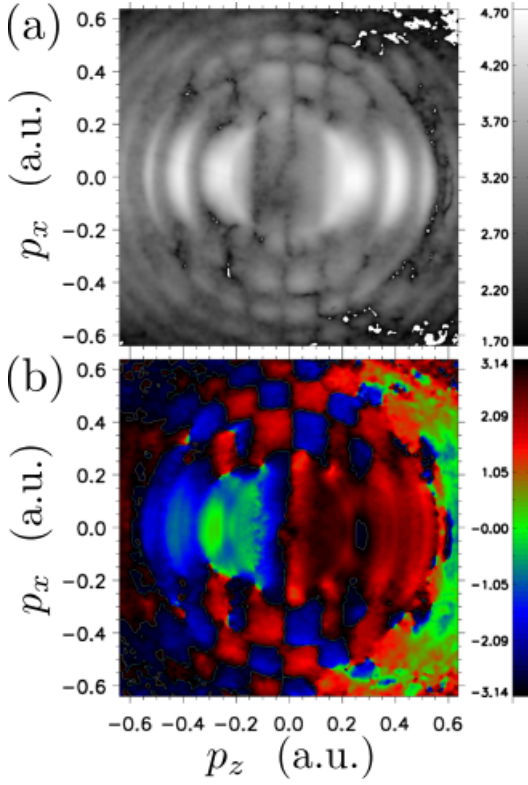


FIG. 2. Experimental RPC $\Delta Y_1(\mathbf{p})$ (a) and PP $\Phi_1(\mathbf{p})$ (b) spectra for Xe. Parameters as for Fig. 1, given in the text. A checkerboard pattern oriented along the ATI rings is visible in the PP spectrum (b).

$|\Psi_0(0)\rangle$ affects the result only as a preexponential form factor $\langle \mathbf{p} + \mathbf{A} | \mathbf{r} | \Psi_0(0) \rangle \cdot \mathbf{E}(t)$ [1, 3]. For simplicity, we chose a hydrogen-like 1s state for $|\Psi_0(0)\rangle$ with I_p adjusted to Xe. For all φ ATI rings are clearly visible. For $\varphi = 0$ (or π), the SFA-PES is left-right symmetric (i.e., invariant under the transformation $p_z \rightarrow -p_z$). Instead, for $\varphi = \pi/2$ and $3\pi/2$ the weak 2ω component of the laser field introduces a visible left-right asymmetry: the ATI peaks appear to be more pronounced and shifted along the ATI rings. These shifts could be reproduced extending the quantum orbit approach and the calculation of the curves of destructive interference as outlined in [28] to two-color fields. However, we aim at a closed analytic expression for the ionization probability as a function of the relative phase in this work and thus follow a different route.

Figure 4 shows the RPC $\Delta Y_1(\mathbf{p})$ and the PP $\Phi_1(\mathbf{p})$ for the parameters of Fig. 3. A checkerboard pattern similar to the one in the experimental PP spectrum in Fig. 2b is observed, at least for sufficiently big lateral momenta $|p_x|$. The PP signature for small momenta is different because of the neglect of Coulomb effects on the emitted electrons in the SFA [3, 30]. The fact that there is a checkerboard pattern in PP spectra at all is simple to understand: if an ATI peak moves along its ATI ring, the yield increases in regions where previously was less probability and decreases at the initial location. As a consequence, only two discrete PPs show up. Why the yield within an SFA treatment behaves $\pm \sin \varphi$ -like and not with

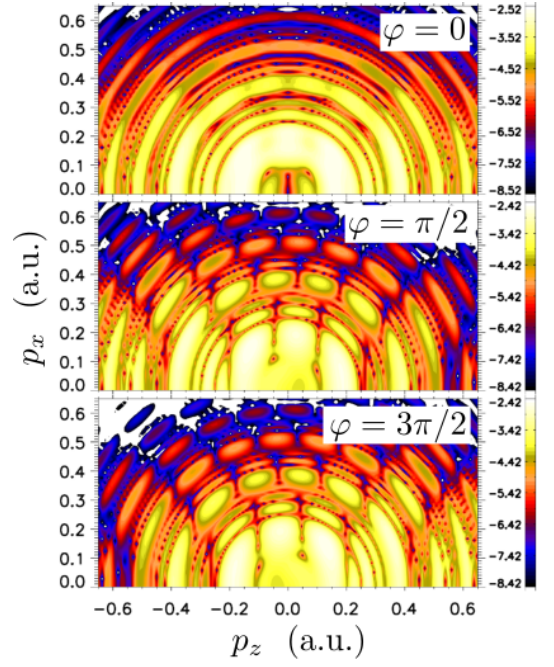


FIG. 3. Logarithmically color-coded SFA-PES for $I_p = 0.445$ (Xe), vector potential amplitude $A_0 = 2/3$, $\omega = 0.057$, 20-cycle \sin^2 pulse, $\xi = 0.05$, and $\varphi = 0, \pi/2, 3\pi/2$, calculated from (3).

some other pair of PPs is less obvious but will be derived analytically in the following.

In order to obtain an analytical result we work in velocity gauge and consider long flat-top pulses of vector potential amplitude A_0 that are switched on and off at $\mp\infty$. It is known that the SFA is plagued by gauge non-invariance, leading, in general, to different PES for velocity gauge (with $\mathbf{p} \cdot \mathbf{A}(t)$ as the interaction term) and length gauge (with $\mathbf{r} \cdot \mathbf{E}(t)$, with the electric field $\mathbf{E} = -\partial_t \mathbf{A}$) [31]. However, in this work we use an 1s-state as the initial state for the SFA and tune the ionization potential I_p to the experimental value. In that case there is no visible difference between length and velocity gauge PES obtained numerically from the SFA. The SFA matrix element relevant for the ionization rate $\Gamma_{\mathbf{p}}$ can then be written in the form [32]

$$M_{\mathbf{p}}^{(\text{SFA})} = i\Psi_0(\mathbf{p}) \left(\frac{p^2}{2} + I_p \right) \int_{-\infty}^{\infty} dt e^{iS_{\mathbf{p}, I_p}(t)}, \quad (6)$$

with $\Psi_0(\mathbf{p}) = \langle \mathbf{p} | \Psi_0 \rangle$ and

$$S_{\mathbf{p}, I_p}(t) = \int_{-\infty}^t \left\{ \frac{1}{2} [\mathbf{p} + \mathbf{A}(t')]^2 + I_p \right\} dt'. \quad (7)$$

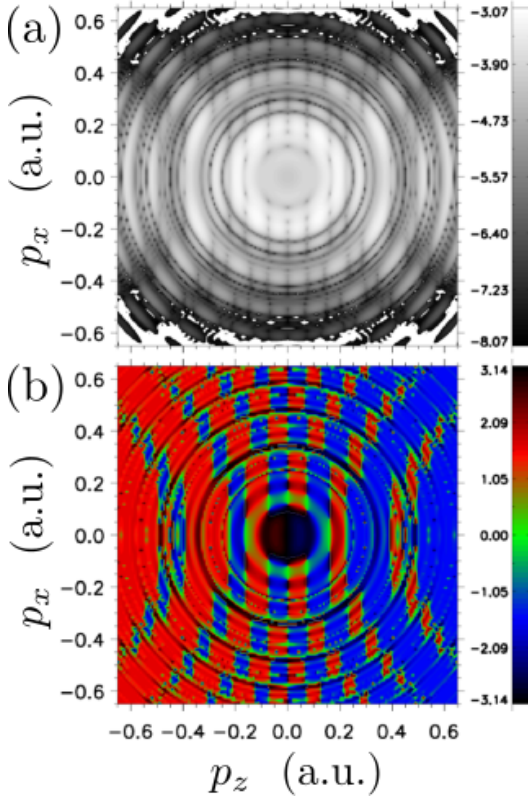


FIG. 4. RPC (a) and PP (b) calculated from PES for 20 values of $\varphi \in [0, 2\pi)$ and the parameters of Fig. 3.

Inserting (1) with $A_0(t) = A_0$ into (7),

$$S_{\mathbf{p}, I_p}(t) = \left(\frac{p^2}{2} + I_p + U_p \right) t - \frac{A_0 p_z}{\omega} \sin(\omega t + \pi/2) + \frac{A_0^2}{8\omega} \sin[2(\omega t + \pi/2)] - \frac{A_0 \xi}{\omega} \left[\frac{p_z}{2} \cos(2\omega t + \varphi) + \frac{A_0}{6} \sin(3\omega t + \varphi) - \frac{A_0}{2} \sin(\omega t + \varphi) \right] + \mathcal{O}(\xi^2) \quad (8)$$

is obtained. Here, $U_p = A_0^2/4$ is the ponderomotive energy. With the help of the generalized Bessel functions $J_n(u, v)$,

$$e^{i[u \sin \phi + v \sin(2\phi)]} = \sum_{n=-\infty}^{\infty} e^{in\phi} J_n(u, v), \quad (9)$$

$$J_n(u, -v) = (-1)^n J_{-n}(u, v), \quad (10)$$

we can evaluate the matrix element (6), neglecting terms of

order $\mathcal{O}(\xi^2)$, as

$$M_{\mathbf{p}}^{(\text{SFA})} = 2\pi i \Psi_0(\mathbf{p}) \left(\frac{p^2}{2} + I_p \right) \times \sum_{n=-\infty}^{\infty} i^n \delta\left(\frac{p^2}{2} + I_p + U_p - n\omega\right) \left\{ J_n + \frac{iA_0\xi}{4\omega} \left[\left(A_0 J_{n+1} + p_z J_{n+2} + \frac{A_0}{3} J_{n+3} \right) e^{i\varphi} + \left(A_0 J_{n-1} + p_z J_{n-2} + \frac{A_0}{3} J_{n-3} \right) e^{-i\varphi} \right] \right\}. \quad (11)$$

Here we suppressed for brevity the arguments of all the generalized Bessel functions, i.e.,

$$J_n = J_n(u, v), \quad u = -\frac{p_z A_0}{\omega}, \quad v = -\frac{U_p}{2\omega}. \quad (12)$$

For the rate follows, analogously to the one-color calculation in, e.g., Refs. [32, 33],

$$\Gamma_{\mathbf{p}} = 2\pi |\psi_0(\mathbf{p})|^2 \left(\frac{p^2}{2} + I_p \right)^2 \times \sum_{n=-\infty}^{\infty} \delta\left(\frac{p^2}{2} + I_p + U_p - n\omega\right) \left\{ J_n^2 - J_n \xi \sin \varphi \times \left[4v(J_{n-1} - J_{n+1}) + \frac{u}{2}(J_{n-2} - J_{n+2}) + \frac{4v}{3}(J_{n-3} - J_{n+3}) \right] \right\}. \quad (13)$$

We can eliminate the terms $\sim J_{n\pm 3}$ using the property of the generalized Bessel functions $2nJ_n = u(J_{n-1} + J_{n+1}) + 2v(J_{n-2} - J_{n+2})$, which yields

$$\Gamma_{\mathbf{p}} = 2\pi |\psi_0(\mathbf{p})|^2 \left(\frac{p^2}{2} + I_p \right)^2 \sum_{n=-\infty}^{\infty} \delta\left(\frac{p^2}{2} + I_p + U_p - n\omega\right) \left[J_n^2 + \Xi_n(u, v) \sin \varphi \right] \quad (14)$$

where

$$\Xi_n(u, v) = -\frac{4\xi J_n}{3} \left[(4v + n)(J_{n-1} - J_{n+1}) - (J_{n-1} + J_{n+1}) - \frac{u}{8}(J_{n-2} - J_{n+2}) \right]. \quad (15)$$

For $\xi = 0$, the known result [32] for the PES without the 2ω component is obtained. The rate (15) has indeed the same structure as the assumed yield in (2), that is

$$\Gamma_{\mathbf{p}} = \Gamma_{0\mathbf{p}} + |\Delta\Gamma_{\mathbf{p}}| \cos[\varphi + \Phi_1(\mathbf{p})], \quad (16)$$

with the RPC $|\Delta\Gamma_{\mathbf{p}}|$ where

$$\Delta\Gamma_{\mathbf{p}} = 2\pi|\psi_0(\mathbf{p})|^2 \left(\frac{p^2}{2} + I_p \right)^2 \times \sum_{n=-\infty}^{\infty} \delta\left(\frac{p^2}{2} + I_p + U_p - n\omega \right) \Xi_n(u, v), \quad (18)$$

and the PP $\Phi_1(\mathbf{p}) = \pm\pi/2$, depending on the sign of $\Delta\Gamma_{\mathbf{p}}$. Evaluating the rate (15) gives very similar results for PP and RPC as in Fig. 4, as shown in Fig. 5. The checkerboard structure is more pronounced in the analytical result because of the flat-top, infinite-pulse assumption on which (15) is based. For the numerical evaluation, the δ distribution in (15) was replaced by a Gaussian $\exp[-(p^2/2 + I_p + U_p - n\omega)^2/a^2]/a\sqrt{\pi}$ with $a = 1/20$, and the sum over n was restricted to $\sum_{n=-30}^{30}$.

IV. DISCUSSION

The characteristic checkerboard pattern in the momentum-resolved phase-of-the-phase spectra is found in both theoretical and experimental results for xenon. As mentioned above, this pattern is related to above-threshold ionization peaks that are shifted with varying relative phase. While the analytical calculation based on the strong-field approximation predicts only $\pm\sin\varphi$ -like behavior of the yield for a $\sin\omega t + \xi\sin(2\omega t + \varphi)$ -like vector potential (1), the experiment shows a more complex PP signature. Also, the experimental relative phase contrast is more oriented along the polarization axis than in the SFA. This clearly points towards the importance of Coulomb effects, which are expected to be the more pronounced the lower the photoelectron energy [30, 34]. Other sources of discrepancy between SFA and experiment are due to focal averaging, the projection onto the VMI detector plane in the measured PES [35], possible resonance-enhanced multiphoton ionization (REMPI) [9] and Freeman resonances [36, 37]. Comparison with PES from the numerical solution of the time-dependent Schrödinger equation will be the subject of future work. Preliminary TDSE results show that the PES also display checkerboard patterns but also PP other than $\pm\sin$ -like, as in the experiment. However, achieving agreement in all details between TDSE and experiment is challenging, even in the case of atomic hydrogen [38].

V. SUMMARY AND OUTLOOK

An analytical expression for the ionization rate in a two-color $(\omega-2\omega)$, colinearly polarized laser field was derived using the strong-field approximation. The change in the yield as a function of the relative phase φ between the two color components was analyzed in the multiphoton regime using the recently introduced phase-of-the-phase spectroscopy. A characteristic checkerboard pattern in the momentum-resolved phase of the phase was found in both theoretical and experimental results for xenon.

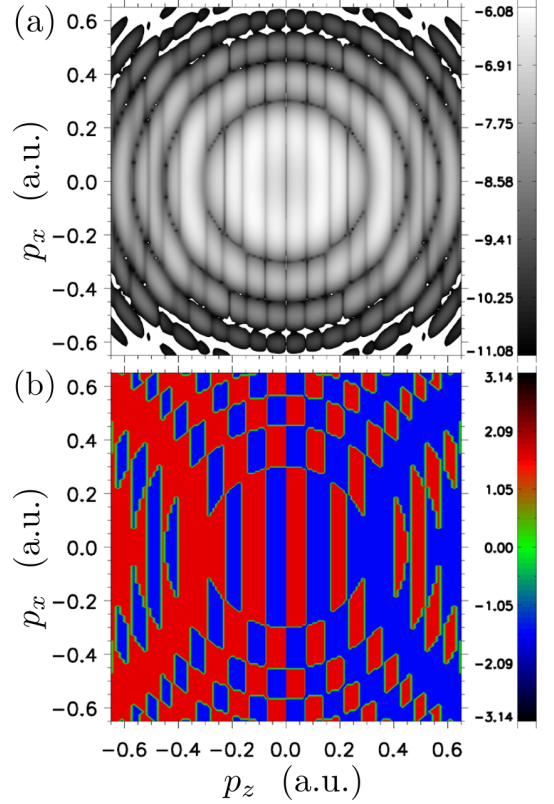


FIG. 5. RPC (a) and PP (b) spectra calculated using the flat-top, infinite pulse SFA result for the rate Eq. (15).

The visibility of the checkerboard pattern in the phase-of-the-phase spectra is clearly related to the presence of above-threshold ionization peaks. Now, imagine an experiment where photoelectron spectra from many-electron systems such as larger molecules, clusters, fullerenes, droplets, nanospheres, or solids are measured. Because of the various relaxation channels, above-threshold ionization peaks or other patterns in photoelectron spectra based on the interference of different electron pathways may be masked by delayed or even thermal electron emission, leading to insipidly Maxwellian-like spectra. Phase-of-the-phase spectroscopy effectively removes these incoherently emitted electrons from the spectrum because incoherent emission is independent of the relative phase. This idea was applied to the electron emission from SiO₂ nanospheres due to the interaction with strong, few-cycle laser fields [29] where the phase-of-phase analysis was performed with respect to the carrier-envelope frequency instead of the relative phase between the two colors in a two-color laser field. Clearly, phase-of-the-phase spectroscopy can be applied with respect to any periodic “knob” that can be controlled in an experiment.

ACKNOWLEDGMENT

This work was supported by the SFB 652 and projects BA 2190/8 and TI 210/7 of the German Science Foundation

(DFG).

-
- [1] D. B. Milošević, G. G. Paulus, D. Bauer, and W. Becker, *Journal of Physics B: Atomic, Molecular and Optical Physics* **39**, R203 (2006).
- [2] N. Delone and V. Kraĭnov, *Multiphoton Processes in Atoms: Second Edition*, Atoms and plasmas (Springer, 2000).
- [3] S. V. Popruzhenko, *Journal of Physics B: Atomic, Molecular and Optical Physics* **47**, 204001 (2014).
- [4] D. G. Arbó, K. L. Ishikawa, K. Schiessl, E. Persson, and J. Burgdörfer, *Phys. Rev. A* **81**, 021403 (2010).
- [5] Y. Huismans, A. Rouzé, A. Gijsbertsen, J. H. Jungmann, A. S. Smolkowska, P. S. W. M. Logman, F. Lépine, C. Cauchy, S. Zamith, T. Marchenko, J. M. Bakker, G. Berden, B. Redlich, A. F. G. van der Meer, H. G. Muller, W. Vermin, K. J. Schafer, M. Spanner, M. Y. Ivanov, O. Smirnova, D. Bauer, S. V. Popruzhenko, and M. J. J. Vrakking, *Science* **331**, 61 (2011).
- [6] Y. Huismans, A. Gijsbertsen, A. S. Smolkowska, J. H. Jungmann, A. Rouzée, P. S. W. M. Logman, F. Lépine, C. Cauchy, S. Zamith, T. Marchenko, J. M. Bakker, G. Berden, B. Redlich, A. F. G. van der Meer, M. Y. Ivanov, T.-M. Yan, D. Bauer, O. Smirnova, and M. J. J. Vrakking, *Phys. Rev. Lett.* **109**, 013002 (2012).
- [7] M. Chini, K. Zhao, and Z. Chang, *Nat. Photon.* **8**, 178 (2014).
- [8] C. I. Blaga, J. Xu, A. D. DiChiara, E. Sistrunk, K. Zhang, P. Agostini, T. A. Miller, L. F. DiMauro, and C. D. Lin, *Nature* **483**, 194 (2012).
- [9] X. Gong, C. Lin, F. He, Q. Song, K. Lin, Q. Ji, W. Zhang, J. Ma, P. Lu, Y. Liu, H. Zeng, W. Yang, and J. Wu, *Phys. Rev. Lett.* **118**, 143203 (2017).
- [10] N. Eicke and M. Lein, *Journal of Modern Optics* **64**, 981 (2017).
- [11] M. Busuladžić, A. Gazibegović-Busuladžić, and D. B. Milošević, *Phys. Rev. A* **95**, 033411 (2017).
- [12] N. V. Vvedenskii, A. N. Zheltukhin, A. A. Silaev, D. V. Knyazeva, N. L. Manakov, A. V. Flegel', and M. V. Frolov, *Quantum Electronics* **46**, 361 (2016).
- [13] L. Zhang, G.-L. Wang, S.-F. Zhao, and X.-X. Zhou, *Physics of Plasmas* **24**, 023116 (2017).
- [14] K. R. Hamilton, H. W. van der Hart, and A. C. Brown, *Phys. Rev. A* **95**, 013408 (2017).
- [15] Q. Song, P. Lu, X. Gong, Q. Ji, K. Lin, W. Zhang, J. Ma, H. Zeng, and J. Wu, *Phys. Rev. A* **95**, 013406 (2017).
- [16] A. Natan, L. J. Zipp, and P. H. Bucksbaum, in *International Conference on Ultrafast Phenomena* (Optical Society of America, 2016) p. UM2B.6.
- [17] Y. Li, Y. Zhou, M. He, M. Li, and P. Lu, *Opt. Express* **24**, 23697 (2016).
- [18] S. Yu, Y. Wang, X. Lai, Y. Huang, W. Quan, and X. Liu, *Phys. Rev. A* **94**, 033418 (2016).
- [19] C. A. Mancuso, K. M. Dorney, D. D. Hickstein, J. L. Chaloupka, J. L. Ellis, F. J. Dollar, R. Knut, P. Grychtol, D. Zusin, C. Gentry, M. Gopalakrishnan, H. C. Kapteyn, and M. M. Murnane, *Phys. Rev. Lett.* **117**, 133201 (2016).
- [20] M. Richter, M. Kunitski, M. Schöffler, T. Jahnke, L. P. H. Schmidt, and R. Dörner, *Phys. Rev. A* **94**, 033416 (2016).
- [21] T. Das and C. Figueira de Morisson Faria, *Phys. Rev. A* **94**, 023406 (2016).
- [22] C. L. M. Petersson, S. Carlström, K. J. Schafer, and J. Mauritsson, *Journal of Physics B: Atomic, Molecular and Optical Physics* **49**, 095002 (2016).
- [23] X. Zheng, M.-M. Liu, H. Xie, P. Ge, M. Li, and Y. Liu, *Phys. Rev. A* **92**, 053422 (2015).
- [24] S. Skruszewicz, J. Tiggesbäumker, K.-H. Meiwes-Broer, M. Arbeiter, T. Fennel, and D. Bauer, *Phys. Rev. Lett.* **115**, 043001 (2015).
- [25] D. G. Arbó, S. Nagele, X.-M. Tong, X. Xie, M. Kitzler, and J. Burgdörfer, *Phys. Rev. A* **89**, 043414 (2014).
- [26] Y. Zhou, C. Huang, A. Tong, Q. Liao, and P. Lu, *Opt. Express* **19**, 2301 (2011).
- [27] S. Skruszewicz, J. Passig, A. Przystawik, N. Truong, M. Köther, J. Tiggesbäumker, and K.-H. Meiwes-Broer, *Int. J. Mass Spectrom.* **365**, 338 (2014).
- [28] P. A. Korneev, S. V. Popruzhenko, S. P. Goreslavski, T.-M. Yan, D. Bauer, W. Becker, M. Kübel, M. F. Kling, C. Rödel, M. Wünsche, and G. G. Paulus, *Phys. Rev. Lett.* **108**, 223601 (2012).
- [29] S. Zherebtsov, F. Süßmann, C. Peltz, J. Plenge, K. J. Betsch, I. Znakovskaya, A. S. Alnaser, N. G. Johnson, M. Kübel, A. Horn, V. Mondes, C. Graf, S. A. Trushin, A. Azzeer, M. J. J. Vrakking, G. G. Paulus, F. Krausz, E. Rühl, T. Fennel, and M. F. Kling, *New Journal of Physics* **14**, 075010 (2012).
- [30] D. Bauer, D. B. Milošević, and W. Becker, *Journal of Modern Optics* **53**, 135 (2006), <http://dx.doi.org/10.1080/09500340500217258>.
- [31] D. Bauer, D. B. Milošević, and W. Becker, *Phys. Rev. A* **72**, 023415 (2005).
- [32] H. R. Reiss, *Phys. Rev. A* **22**, 1786 (1980).
- [33] P. Mulser and D. Bauer, *High Power Laser-Matter Interaction*, Springer Tracts in Modern Physics, Vol. 238 (Springer-Verlag Berlin Heidelberg, 2010).
- [34] S. Popruzhenko and D. Bauer, *Journal of Modern Optics* **55**, 2573 (2008).
- [35] M. J. J. Vrakking, *Review of Scientific Instruments* **72**, 4084 (2001).
- [36] R. R. Freeman and P. H. Bucksbaum, *Journal of Physics B: Atomic, Molecular and Optical Physics* **24**, 325 (1991).
- [37] V. Schyja, T. Lang, and H. Helm, *Phys. Rev. A* **57**, 3692 (1998).
- [38] D. Kielpinski, R. T. Sang, and I. V. Litvinyuk, *Journal of Physics B: Atomic, Molecular and Optical Physics* **47**, 204003 (2014).